Solution of Axisymmetric Flame Deconvolution Problems using Tikhonov Auto-Regularization

K. J. Daun and K. A. Thomson
Institute for Chemical Process and Environmental Technology
National Research Council of Canada

Submitted to the Inverse Problems in Engineering Seminar
Ames, Iowa, July 26-27, 2006.

Abstract

When deconvolving data collected in experiments involving axisymmetric flames, small errors that contaminate the data are magnified into large errors in the recovered distribution. This effect can be mitigated by applying Tikhonov regularization, although a regularization parameter must first be chosen that is large enough to suppress error amplification, but not so large that it pushes the regularized solution from the unperturbed "exact" solution. The regularization parameter is usually selected by trial-and-error, a time-consuming procedure that demands specialized mathematical knowledge on the part of the analyst.

This paper describes two algorithms that automatically select the regularization parameter based on the estimated magnitude of the errors that contaminate the measured data. The first algorithm requires the analyst to specify this quantity, usually based on the results of repeated experimental trials, while the second algorithm estimates the error in the dataset using truncated singular value decomposition. The solutions found using these algorithms are more accurate than those obtained by onion-peeling and Abel three-point deconvolution alone. Furthermore, since these algorithms select the Tikhonov regularization parameter automatically, deconvolution is carried out quickly and efficiently without requiring any specialized knowledge of inverse techniques on the part of the analyst.

Nomenclature

$\mathbf{A}$	Coefficient matrix
$\mathbf{A}_{\mathrm{OP}}$	Onion-peeling coefficient matrix
$\mathbf{A}_{\lambda}$	Augmented Tikhonov matrix
$\boldsymbol{b}$	Vector containing projected data
$\boldsymbol{b}^{pert}$	Vector containing perturbed projected data
$\boldsymbol{b}_{\lambda}$	Augmented Tikhonov RHS vector
$f(r)$	Field variable distribution
$f_{exact}(r)$	Exact (unperturbed) field variable distribution
$\mathbf{L}$	Tikhonov smoothing matrix, Eq. (12)
N	Number of annular elements
$P(y)$	Projected data
p	Useful rank of $\mathbf{A}_{\mathrm{OP}}$
$\mathbf{U}$	Orthogonal matrix obtained by SVD
$\boldsymbol{u}_j^T$	*jth* row of $\mathbf{U}^T$
r	Radial location
R	Flame radius
$\mathbf{S}$	Diagonal matrix of singular values
s_j	*jth* singular value
$\mathbf{V}$	Orthogonal matrix obtained by SVD
$\boldsymbol{v}_j$	*jth* row of $\mathbf{V}$
$\boldsymbol{x}$	Vector containing field distribution data
$\widetilde{\boldsymbol{x}}$	Smoothed solution obtained using TSVD, Eq. (17)
$\boldsymbol{x}^{pert}$	Vector containing perturbed field distribution data
y	Axial location
Δr	Thickness of an annular element
$\boldsymbol{\delta b}$	Perturbation vector of $\boldsymbol{b}^{pert}$, $\boldsymbol{\delta b} = \boldsymbol{b}^{pert} - \boldsymbol{b}$
$\boldsymbol{\delta x}$	Perturbation vector of $\boldsymbol{x}^{pert}$, $\boldsymbol{\delta x} = \boldsymbol{x}^{pert} - \boldsymbol{x}$
$\varepsilon_{reg}(\lambda)$	Regularization error in the Tikhonov solution

$\varepsilon_{pert}(\lambda)$	Perturbation error in the Tikhonov solution
$\varepsilon_{\mathrm{RMS}}$	Root-mean-squared error of the deconvolved solution
$\varepsilon_{tot}(\lambda)$	Total error in Tikhonov solution
$\kappa_\lambda(r)$	Extinction coefficient [m^{-1}]
λ	Tikhonov regularization parameter
λ_{AR1}	λ found using replication-based technique
λ_{AR2}	λ found using TSVD-based technique
λ^*	Minimizer of $\varepsilon_{tot}(\lambda)$
$\lambda^\dagger$	Minimizer of $\varepsilon_{reg}(\lambda) + \varepsilon_{pert}(\lambda)$
σ	Standard deviation of projected data
σ_m	Standard deviation of the mean

Introduction

The objective of many combustion experiments involving axisymmetric flames is to infer the distribution of a property within the flame field from optical measurements made through the flame. For example, in line-of-sight-attenuation (LOSA) experiments light attenuation measurements made through the flame are used to reconstruct the radial extinction coefficient distributions, as shown schematically in Fig. 1 (*a*). In a second example, emission tomography, the temperature distribution within the flame field is inferred from radiant intensity measurements taken at various locations outside of the flame. In both experiments, optical data measured along a set of chord lines passing through the flame field, called the *projected data*, $P(y)$, are deconvolved to recover the radial distribution of a *field variable*, $f(r)$, over the range $0 \le r \le R$. These two variables are related by Abel's integral equation,

$$P(y) = 2\int_{y}^{R} \frac{f(r)\,r}{\sqrt{r^2 - y^2}}\,dr\,, \tag{1}$$

which is a type of Volterra integral equation of the first kind, a class of equations that are moderately ill-posed.

Unlike many integral equations of the first-kind, Eq. (1) has an analytical solution,

$$f(r) = \frac{-1}{\pi}\int_{y}^{R} \frac{P'(y)}{\sqrt{y^2 - r^2}}\,dy, \tag{2}$$

where $P'(y) = dP/dy$. This solution is of limited use, however, since projected data is not known as a continuous function of y, but only at a discrete set of axial locations. Furthermore, approximating the derivative using finite differences methods amplifies

experimental error contaminating the projected dataset to unacceptable levels, particularly since the integrand of Eq. (2) becomes singular as y approaches r. (This is, in fact, a symptom of the ill-posed nature of Abel's integral equation.)

Although the analytical forms of Eq. (1) and (2) cannot be used to obtain $f(r)$ directly, they are the foundation for the two most popular deconvolution methods used by combustion researchers. In onion-peeling, the integral domain is split into N evenly-spaced segments, which is equivalent to discretizing the flame field into N uniformly-spaced annular elements that have a radial thickness $\Delta r = R/(N-1/2)$ as shown in Fig. 1 (*b*). Once this is done, the field variable is assumed to be uniform over each sub-domain of r and is extracted from the integral, leaving

$$P_i \approx 2\sum_{j=i}^{N-1} f_j \int_{\substack{r_j-\Delta r/2 \\ r_j, j=i}}^{r_j+\Delta r/2} \frac{r}{\sqrt{r^2 - y_i^2}}\, dr,\ i = 0, 1, \ldots, N, \tag{3}$$

where $y_i = i\Delta r$, $r_j = j\Delta r$, $P_i = P(y_i)$ and $f_j = f(r_j)$. Writing Eq. (3) for every projection and carrying out the integrals results in a matrix equation $\mathbf{A}_{\mathrm{OP}}\boldsymbol{x} = \boldsymbol{b}$, where $x_i = f(r_i)$, $b_i = P(y_i)$, and

$$A_{\mathrm{OP},ij} = \begin{cases} 0, & j < i \\ 2\Delta r\sqrt{\left(j+\tfrac{1}{2}\right)^2 - i^2}, & j = i \\ 2\Delta r\left[\sqrt{\left(j+\tfrac{1}{2}\right)^2 - i^2} - \sqrt{\left(j-\tfrac{1}{2}\right)^2 - i^2}\right], & j > i. \end{cases} \tag{4}$$

The element $A_{\mathrm{OP},ij}$ represents the contribution of $f(r_j)$ to the projected variable $P(y_i)$, and is equal to the length of the chord passing through y_i that lies in the *jth* annular element.

An alternative way of solving for $f(r)$ is through Abel three-point deconvolution. As in the previous method, the first step in this approach is to discretize the flame field

into N equally-spaced annular elements, which is equivalent to splitting the integral of Eq. (2) into N sub-domains,

$$f_i = \frac{-1}{\pi}\sum_{j=i}^{N-1}\int_{\substack{y_i,\,j=i\\ y_j-\Delta r/2,\,j>i}}^{y_j+\Delta r/2}\frac{P'(y)}{\sqrt{y^2-r_i^2}}dy, i=0,1,\ldots,N. \tag{5}$$

A subset of the projected dataset is used to define an interpolating quadratic spline that approximates $P(y)$ over each sub-domain, with $\{P_{j-1}, P_j, P_{j+1}\}$ used over the *jth* domain, $y_j-\Delta r/2 \le y \le y_j+\Delta r/2$. (At $j = 0$, $P_{-1} = P_1$, and at $j = N-1$, $P_N = 0$, in order to satisfy $P'(0) = 0$ and $P(R) = 0$, respectively.) These quadratic splines are then differentiated with respect to y and substituted into Eq. (5). Carrying out the integration results in an explicit expression for each f_i in terms of the projected data, $\{P_j, j = i, i+1, \ldots, N-1\}$. Dasch [1] provides a more complete description of both onion-peeling and Abel three-point deconvolution methods.

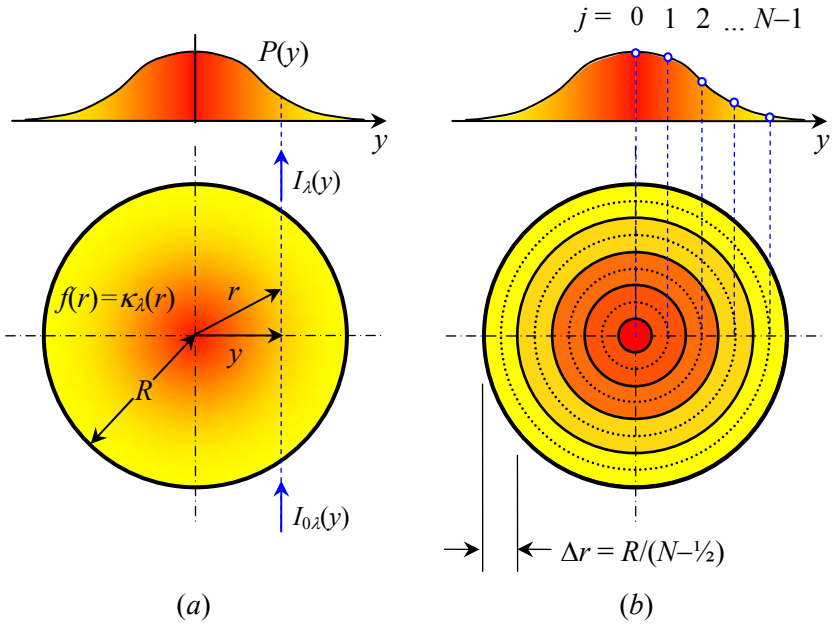

Fig. 1: (*a*) LOSA axisymmetric flame deconvolution problem, and (*b*) discretization of the problem domain.

Both onion-peeling and Abel-three-point deconvolution provide accurate solutions for $f(r)$ when the exact projected data is known. In an experimental setting, however, the projected dataset is inevitably contaminated with small errors that are magnified by deconvolution into large errors in the recovered field variable distribution. This is a consequence of the fundamental ill-posed nature of Abel's integral equation and is exacerbated as N increases for both onion-peeling and Abel three-point inversion, severely limiting the deconvolved field variable resolution.

This effect can be mitigated by using a regularization technique to perform the deconvolution. These techniques work by transforming the original ill-posed problem into a set of better-posed, or *regularized*, problems. Regularized problems that closely resemble the original ill-posed problem are themselves ill-posed, having solutions that solve the original problem with a very small residual but are also highly sensitive to small perturbations in the problem parameters. Using more regularization improves the solution stability, but at the expense of solution accuracy. The degree of regularization is controlled by a *regularization parameter*, which is adjusted until an acceptable trade-off between solution accuracy and stability is found. Both onion-peeling and Abel three-point inversion are regularization methods in their own right, where the regularization parameter is the number of annular elements used to solve the problem, N. In both cases, using fewer annular elements (and few projections) produces solutions that are more resilient to errors in the projected dataset, but do not accurately represent the actual field variable distribution, particularly in regions where $f(r)$ changes rapidly. The solution becomes more accurate as N increases, but also becomes more sensitive to perturbations in the projected data. These algorithms do not provide adequate control over the level of

regularization used to perform the deconvolution, however, since N is not easily adjusted to account for different levels of error contamination in the projected dataset and different field variable distributions, both of which affect the degree of error amplification caused by deconvolution.

In a recent work [2], we showed that Tikhonov regularization [3] is a better choice for a regularization technique. In this approach the ill-conditioned matrix equation obtained by onion-peeling, $\mathbf{A}_{OP}\boldsymbol{x} = \boldsymbol{b}$, is augmented with a homogeneous system of regularizing equations $\lambda\mathbf{L}\boldsymbol{x} = 0$, where $\mathbf{L}$ is a smoothing matrix and λ is a continuously-variable regularization parameter. In our previous paper [2] we showed that λ can be adjusted with high fidelity until a near-optimum trade-off between accuracy and solution stability is found, for a specified field distribution, level of discretization, and degree of error contamination.

The most critical and difficult part of the above procedure lies in selecting the appropriate regularization parameter. This is usually done heuristically, by examining the recovered field-variable distributions obtained using different values of λ and selecting one that is just large enough to suppress perturbations in $f(r)$ due to error contamination in the projected data, but is not so large that it pushes the regularized solution too far away from the unperturbed solution. This trial-and-error procedure is time consuming and requires specialized knowledge and experience on the part of the analyst.

The objective of this paper is to present techniques that choose λ automatically, thereby making Tikhonov regularization easier and less time-consuming to implement, particularly for researchers who are not familiar with regularization. We first review the

ill-posed nature of Abel's integral equation and how Tikhonov regularization is applied to solve this problem. Next, we present two algorithms that choose the regularization parameter automatically. The first algorithm can be used when a good estimate of the contamination of the projected dataset is available, most often by performing repeated experimental trials. The second technique, recently developed by Jones [4], uses truncated singular value decomposition (TSVD) [5] to estimate the contamination of the projected data automatically, which in turn is used to select the appropriate level of regularization. The performance of both algorithms is demonstrated and compared to that of onion-peeling and Abel three-point deconvolution by solving a problem inspired by a recent experimental LOSA study [6].

The Ill-Posed Nature of Abel's Integral Equation

The formal definition of what constitutes a mathematically ill-posed problem is attributed to Hadamard [7], who classified mathematically well-posed problems as those that have a unique solution that is insensitive to small changes to the problem parameters. By inference, a mathematically ill-posed problem is one that either does not have a solution, has multiple solutions, or has a solution that is highly sensitive to small perturbations in the problem definition. The flame deconvolution problem obviously has at least one solution, that being the field variable distribution that produced the experimentally-observed projected data. Furthermore, it can also be shown mathematically that Abel's equation only admits one unique solution [8]. This can also be reasoned physically since the integral domain in Eq. (1) approaches zero as $r \rightarrow R$, and $f(R)$ is thus known with

certainty; a unique $f(r)$ is then calculated from the outside-in, in an analogy to onion-peeling in continuous space.

Instead, Abel's integral equation is ill-posed because it violates Hadamard's third criterion of well-posed problems, i.e. small perturbations in the problem definition (in this case experimental error contaminating the projected dataset) are magnified into large perturbations in the solution by the deconvolution process. The mechanism by which this occurs is demonstrated mathematically by applying singular value decomposition (SVD) [5] to the onion-peeling matrix. In this procedure, $\mathbf{A}_{\mathrm{OP}}$ is factored into $\mathbf{U}\cdot\mathbf{S}\cdot\mathbf{V}^T$, where $\mathbf{U}$ and $\mathbf{V}$ are $N \times N$ orthogonal matrices and $\mathbf{S}$ is a diagonal matrix of singular values. (SVD can also be used to factor and solve rectangular matrix equations, which is done later in this paper.) Because $\mathbf{U}$ and $\mathbf{V}$ are orthogonal, it is easy to rewrite $\mathbf{A}_{\mathrm{OP}}\boldsymbol{x} = \boldsymbol{b}$ as

$$\boldsymbol{x} = \mathbf{V}\mathbf{S}^{-1}\left(\mathbf{U}^T\boldsymbol{b}\right), \tag{6}$$

or

$$\boldsymbol{x} = \sum_{j=1}^{N} \frac{\boldsymbol{u}_j^T\boldsymbol{b}}{s_j}\boldsymbol{v}_j, \tag{7}$$

where $\boldsymbol{u}_j^T$ and $\boldsymbol{v}_j$ are the jth rows of $\mathbf{U}^T$ and $\mathbf{V}$, and $s_j = S_{jj}$ is the jth singular value. If the projected dataset is uncontaminated, Eq. (7) can be used to calculate the exact field variable distribution directly. If a perturbation vector $\boldsymbol{\delta b}$ is added to the projected data contained in $\boldsymbol{b}$, however, the SVD back-substitution returns a perturbed solution $\boldsymbol{x}^{pert} = \boldsymbol{x}+\boldsymbol{\delta x}$

$$\boldsymbol{x}^{pert} = \sum_{j=1}^{N} \frac{\boldsymbol{u}_j^T\left(\boldsymbol{b}+\boldsymbol{\delta b}\right)}{s_j}\boldsymbol{v}_j = \sum_{j=1}^{N} \frac{\boldsymbol{u}_j^T\boldsymbol{b}^{pert}}{s_j}\boldsymbol{v}_j, \tag{8}$$

The errors in the deconvolved field variable are amplified when, for some terms in the summation of Eq. (8), $\boldsymbol{u}_j^T\boldsymbol{\delta b}$ approaches the magnitude of $\boldsymbol{u}_j^T\boldsymbol{b}$ when s_j is small. This scenario is described in more detail in [4].

This situation is demonstrated for the first of two deconvolution test distributions, $f_1(r)$ and $f_2(r)$, as shown in Fig. 2. The field variables were derived by least-squares fitting 4$^{\text{th}}$-order piecewise polynomials to two different sets of normalized soot-volume fraction data obtained from LOSA experiments carried out on high-pressure laminar flames [6]. The right-hand side vector, $\boldsymbol{b}$, which contains the projected data, was then calculated by analytically integrating Eq. (1). The elements of the perturbation vector, $\boldsymbol{\delta b}$, were randomly-sampled from an unbiased Gaussian distribution having a standard deviation of 0.01, which is typical of experimental error encountered in LOSA flame experiments [6]. Figure 3 shows the solution to the first test problem obtained by deconvolving perturbed projected data using onion-peeling and Abel three-point deconvolution with N = 50, clearly demonstrating that small perturbations in the projected data are amplified by both deconvolution processes into large perturbations in the solution, $\boldsymbol{\delta x}$.

This amplification mechanism becomes evident when Eq. (8) is used to reconstruct $\boldsymbol{x}^{pert}$; the corresponding singular values of $\mathbf{A}_{\text{OP}}$ as well as $\boldsymbol{u}_j^T\boldsymbol{b}/s_j$ and $\boldsymbol{u}_j^T\boldsymbol{\delta b}/s_j$ are plotted in Fig. 4. At small values of j, $\boldsymbol{u}_j^T\boldsymbol{b}$ is much larger than $\boldsymbol{u}_j^T\boldsymbol{\delta b}$, and the corresponding terms in the summation are unaffected by the perturbation. At a critical value of j, however, the terms in the numerator, $\boldsymbol{u}_j^T\boldsymbol{b}$ and $\boldsymbol{u}_j^T\boldsymbol{\delta b}$, are similar in magnitude and s_j is very small, thereby amplifying the influence of the perturbations on the deconvolved field distribution.

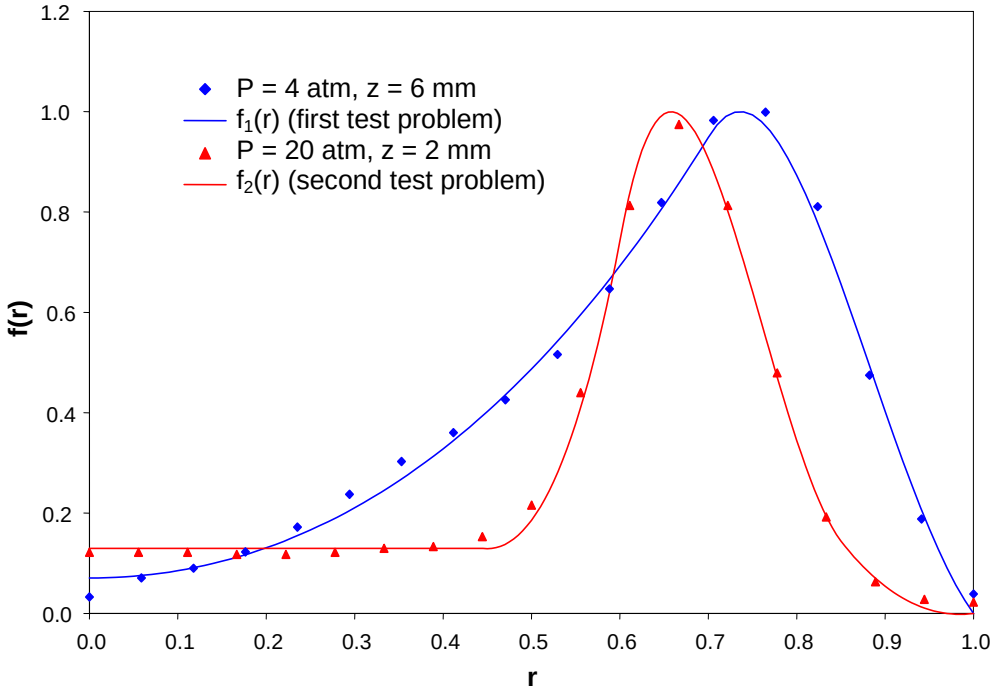

Fig. 2: Normalized experimental data [6] and fitted field variable test distributions.

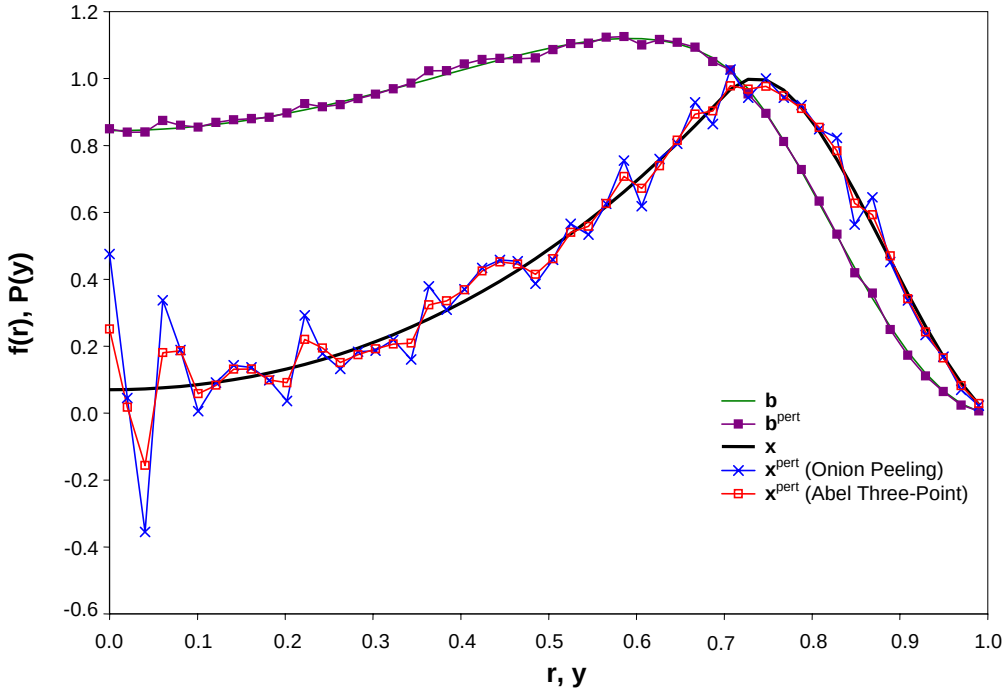

Fig. 3: Projected data and field distributions recovered by onion-peeling and Abel three-point deconvolution for $f_1(r)$.

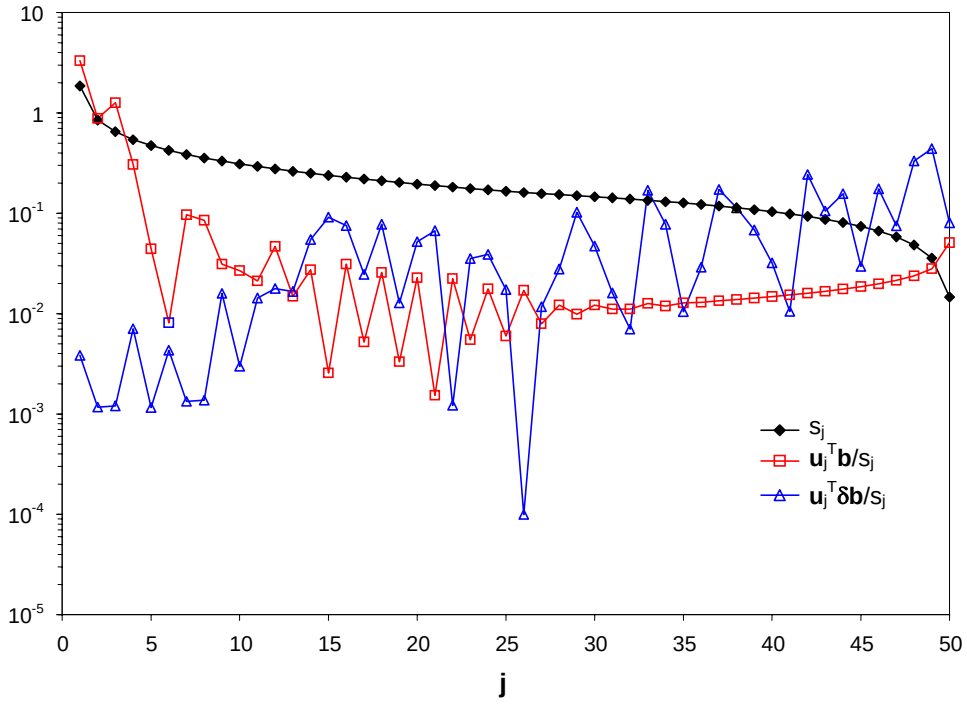

Fig. 4: Singular values of $\mathbf{A}_{OP}$ and back-substitution summation terms from Eq. (8) for $f_1(r)$.

Tikhonov Regularization

The perturbation amplification mechanism described above can be suppressed using Tikhonov regularization [3]. Tikhonov regularization is best understood by first observing that solving $\mathbf{A}\boldsymbol{x} = \boldsymbol{b}$ is equivalent to finding the value $\boldsymbol{x}^*$ that minimizes

$$F(\boldsymbol{x}) = \frac{1}{2}\boldsymbol{x}^T\mathbf{A}^T\mathbf{A}\boldsymbol{x} - \boldsymbol{x}^T\mathbf{A}^T\boldsymbol{b}. \tag{9}$$

If $\mathbf{A}$ is well-conditioned, $F(\boldsymbol{x})$ has a unique and well-defined local minimum. If $\mathbf{A}$ is ill-conditioned, on the other hand, $F(\boldsymbol{x})$ is nearly degenerate; in other words, $\boldsymbol{x}^*$ lies at the bottom of a long, shallow valley and many potential solutions $\boldsymbol{x}^{pert} = \boldsymbol{x} + \delta\boldsymbol{x}$ that lie along the valley floor satisfy the matrix equation with a small residual, $\boldsymbol{b}^{pert} = \boldsymbol{b} + \delta\boldsymbol{b}$. This scenario is shown in Fig. 5 (*a*) for the linear system $\mathbf{A}\boldsymbol{x} = \boldsymbol{b}$ with $\mathbf{A} = [(4, 2.5), (2, 1)]^T$ and $\boldsymbol{b} = [-4, -2]^T$. The points plotted in Fig. 5 (*a*) are solutions of $\mathbf{A}\boldsymbol{x}^{pert} = \boldsymbol{b}^{pert}$ where $\delta\boldsymbol{b}$ is a randomly-generated perturbation vector that satisfies $\|\delta\boldsymbol{b}\|_2 < 0.283$.

In Tikhonov regularization a second function, $\frac{1}{2}\lambda^2\boldsymbol{x}^T\mathbf{L}^T\mathbf{L}\boldsymbol{x}$, is added to $F(\boldsymbol{x})$ to make it less degenerate, i.e. to make the valley floor steeper in the vicinity of $\boldsymbol{x}^*$. In this composite objective function, $F_{Tik}(\boldsymbol{x}) = F(\boldsymbol{x}) + \frac{1}{2}\lambda^2\boldsymbol{x}^T\mathbf{L}^T\mathbf{L}\boldsymbol{x}$, λ is the regularization parameter and $\mathbf{L}$ is a smoothing matrix, which in this problem is an $(N - 1 \times N)$ matrix that approximates the derivative operator in discrete space [9],

$$\mathbf{L} = \begin{bmatrix} 1 & -1 & 0 & \cdots & & 0 \\ 0 & 1 & -1 & \ddots & & \vdots \\ \vdots & \ddots & \ddots & \ddots & & \\ & & & 1 & -1 & 0 \\ 0 & \cdots & & 0 & 1 & -1 \end{bmatrix}. \tag{10}$$

The value of $\boldsymbol{x}$ that minimizes $F_{Tik}(\boldsymbol{x})$, $\boldsymbol{x}_\lambda$, also minimizes the residual of the augmented matrix equation $\mathbf{A}_\lambda\boldsymbol{x} = \boldsymbol{b}_\lambda$, i.e.

$$\left\|\mathbf{A}_\lambda \boldsymbol{x}_\lambda - \boldsymbol{b}_\lambda\right\|_2 = Min_x\left[\left\|\mathbf{A}_\lambda \boldsymbol{x} - \boldsymbol{b}_\lambda\right\|_2\right] = Min_x\left\{\left\|\begin{bmatrix}\mathbf{A}\\ \lambda\mathbf{L}\end{bmatrix}\boldsymbol{x} - \begin{bmatrix}\boldsymbol{b}\\ 0\end{bmatrix}\right\|\right\}, \tag{11}$$

and can be found efficiently by solving

$$\left(\mathbf{A}_{\mathrm{OP}}^T\mathbf{A}_{\mathrm{OP}}^T + \lambda^2\mathbf{L}^T\mathbf{L}\right)\boldsymbol{x}_\lambda = \mathbf{A}_{\mathrm{OP}}^T\boldsymbol{b}. \tag{12}$$

As shown in Fig. 5 (*b*-*d*), increasing λ "steepens" the objective function topography and decreases the spread of perturbed solutions. At the same time, however, increasing λ also shifts $\boldsymbol{x}_\lambda$ away from solution of the original problem, $\mathbf{A}\boldsymbol{x} = \boldsymbol{b}$.

The effect of increasing λ can also be seen in the singular value spectra of $\mathbf{A}_\lambda$, which is plotted in Fig. 6 for the case in which $\mathbf{A}_{\mathrm{OP}}$ (N = 50) is substituted for $\mathbf{A}$ in the augmented matrix equation. (The N–1 null singular values corresponding to the nullity of $\mathbf{A}_\lambda$ are not shown in Fig. 6 and are also excluded when reconstructing $\boldsymbol{x}$ using Eq. (8).) Increasing λ increases the small singular values that amplify $\delta\boldsymbol{b}$, thereby suppressing the influence of these terms in the summation of Eq. (8). This, in turn, reduces the perturbations in the deconvolved field distribution, as shown in Fig. 7 for the first LOSA test problem described above with $\|\delta\boldsymbol{b}\|_2 < 0.01$. If λ is too large, however, the singular value spectrum is excessively modified and the corresponding regularized solution is pushed away from the unperturbed "exact" solution.

Both of the above examples demonstrate that while increasing λ reduces the magnitude of perturbations in the solution, it also pushes the regularized solution away from the unperturbed solution. The amount of regularization must therefore be carefully selected to obtain an acceptable trade-off between smoothness and accuracy; strategies for doing this are presented in the next section.

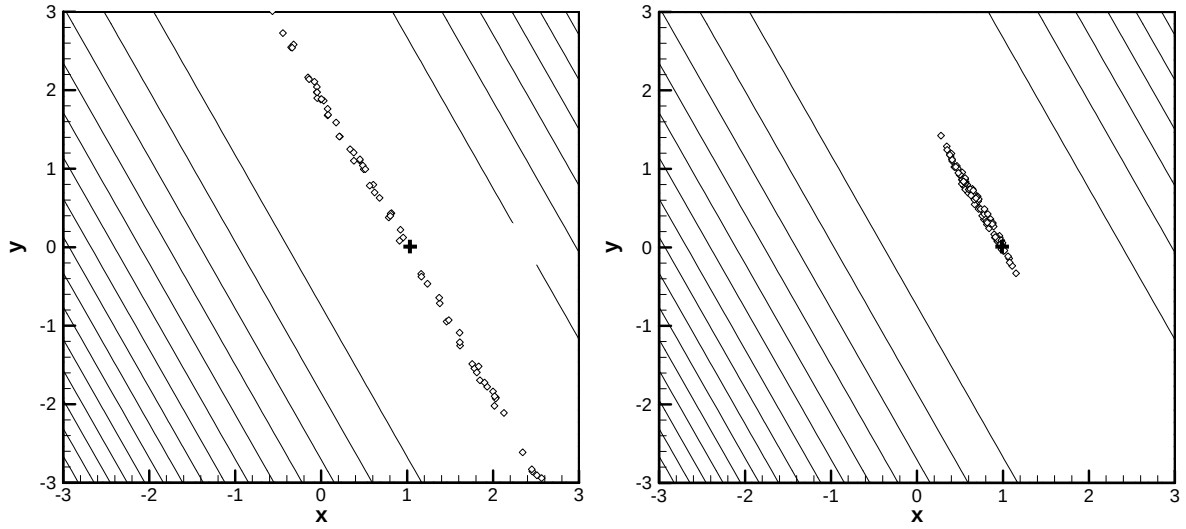

(*a*) $\lambda = 0$ (*b*) $\lambda = 5 \times 10^{-3}$

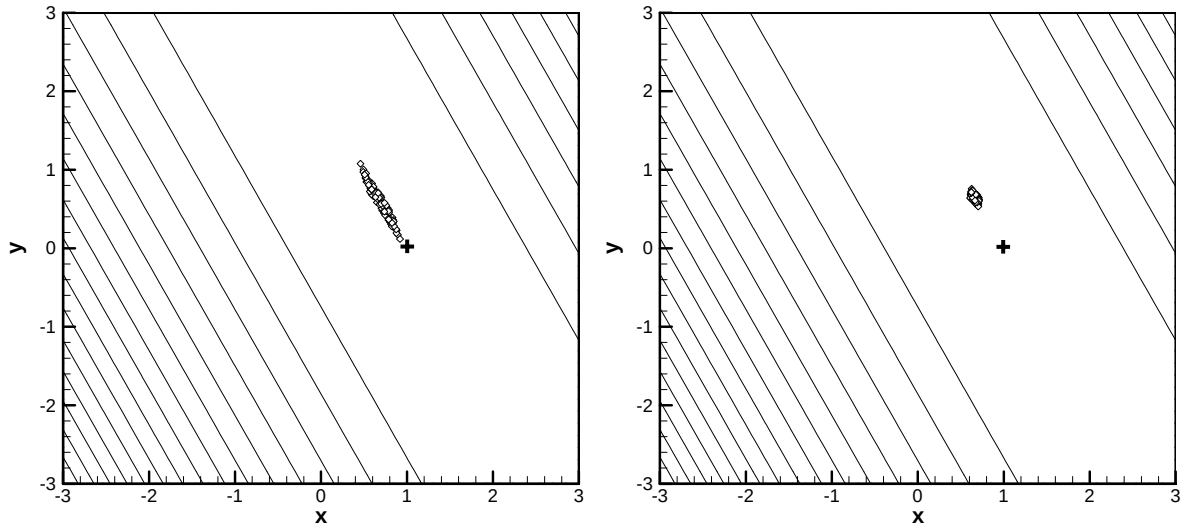

(*c*) $\lambda = 10^{-2}$ (*d*) $\lambda = 5 \times 10^{-2}$

Fig. 5: Plots of $F_{tik}(\boldsymbol{x}) = 1/2 \cdot \boldsymbol{x}^T(\mathbf{A}^T\mathbf{A}+\lambda^2\mathbf{L}^T\mathbf{L})\boldsymbol{x} - \boldsymbol{b}^T\mathbf{A}\boldsymbol{x}$ for different amounts of regularization, with $\mathbf{A} = \{(4, 2.5), (2, 1)\}^T$ and $\boldsymbol{b} = \{-4, -2\}^T$. The analytical solution, $\boldsymbol{x}$, is marked with a cross, while diamonds denote values of $\boldsymbol{x}_\lambda^{pert}$ obtained by contaminating $\boldsymbol{b}$ with a perturbation vector that satisfies $||\boldsymbol{\delta b}||_2 < 0.283$.

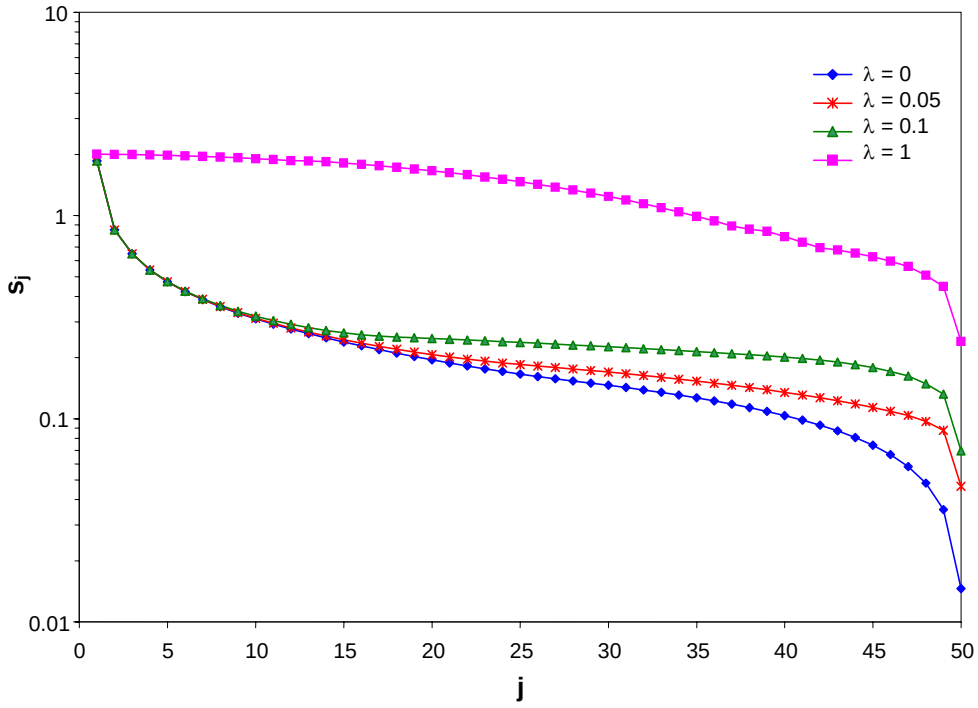

Fig. 6: Singular value spectra of $\mathbf{A}_\lambda$ using different levels of regularization for the first test problem. (Null singular values are not shown.)

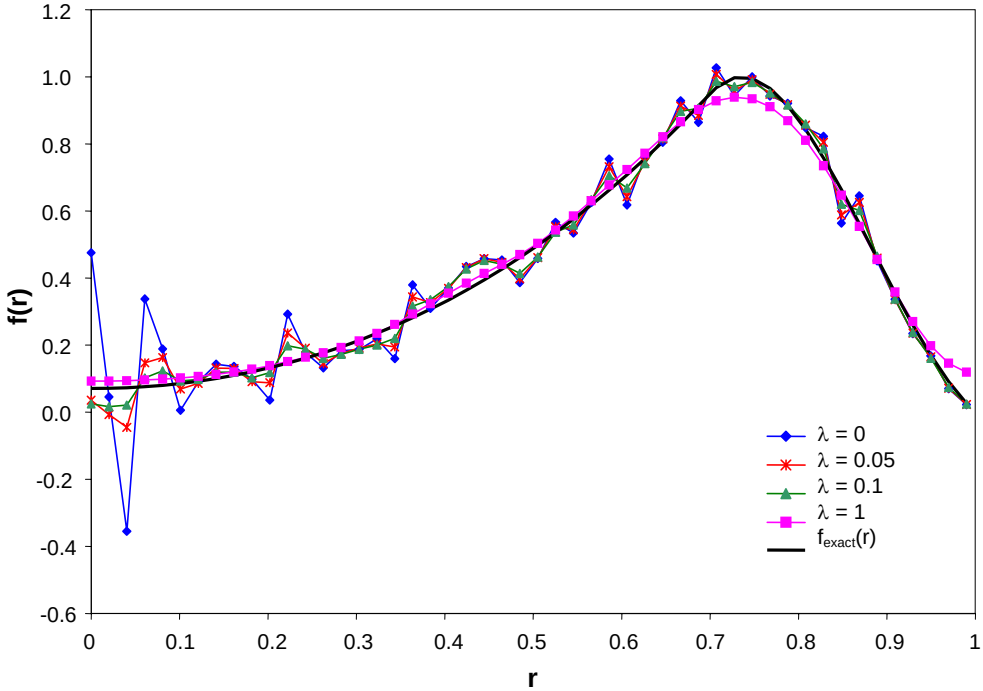

Fig. 7: Deconvolved field distributions for the first test problem obtained by applying Tikhonov regularization to $\mathbf{A}_{OP}(N=50)$, using different levels of regularization.

Strategies for Selecting the Regularization Parameter

When selecting the regularization parameter, the goal is to minimize the overall solution error, which is due to both the contamination of the projected data and to the regularization process. More formally, the total error is written as [5]

$$\boldsymbol{x} - \boldsymbol{x}_\lambda^{pert} = \mathbf{A}_{\mathrm{OP}}^{-1}\boldsymbol{b} - \mathbf{A}_\lambda^{-1}\boldsymbol{b}^{pert} = \left(\mathbf{A}_{\mathrm{OP}}^{-1} - \mathbf{A}_\lambda^{-1}\right)\boldsymbol{b} - \mathbf{A}_\lambda^{-1}\boldsymbol{\delta b}, \tag{13}$$

where $\boldsymbol{x}$ denotes the exact, unperturbed solution, $\boldsymbol{x}_\lambda^{pert}$ is the regularized solution of the perturbed matrix equation, and $\mathbf{A}_{\mathrm{OP}}^{-1}$ and $\mathbf{A}_\lambda^{-1}$ are the pseudoinverses of the onion-peeling and augmented matrices, respectively. (Taking the pseudoinverse of $\mathbf{A}_\lambda$ removes its (N–1)-dimension null-space, thereby making $\mathbf{A}_\lambda^{-1}$ compatible with $\boldsymbol{b}$ and $\boldsymbol{\delta b}$.) The total error is more easily quantified by taking the l_2-norm of the vectors in Eq. (13),

$$\varepsilon_{tot}(\lambda) = \left\|\boldsymbol{x} - \boldsymbol{x}_\lambda^{pert}\right\|_2 \le \left\|\left(\mathbf{A}_{OP}^{-1} - \mathbf{A}_\lambda^{-1}\right)\boldsymbol{b}\right\|_2 + \left\|\mathbf{A}_\lambda^{-1}\boldsymbol{\delta b}\right\|_2 = \varepsilon_{reg}(\lambda) + \varepsilon_{pert}(\lambda), \tag{14}$$

where $\varepsilon_{reg}(\lambda)$ is the regularization error and $\varepsilon_{pert}(\lambda)$ is the perturbation error. As demonstrated above, increasing λ suppresses the magnification of $\boldsymbol{\delta b}$ and decreases $\varepsilon_{pert}(\lambda)$, but this also increases the $\varepsilon_{reg}(\lambda)$ since $\lambda\mathbf{L}$ obscures $\mathbf{A}_{\mathrm{OP}}$ in the augmented matrix $\mathbf{A}_\lambda$ as λ becomes large. Thus, a value of λ must be chosen that is an acceptable trade-off between $\varepsilon_{pert}(\lambda)$ and $\varepsilon_{reg}(\lambda)$.

Most often, λ is selected heuristically with the aid of an L-curve, a plot of the smoothed solution norm, $\left\|\mathbf{L}\boldsymbol{x}_\lambda^{pert}\right\|_2$, against the residual norm, $\left\|\mathbf{A}_{\mathrm{OP}}\boldsymbol{x}_\lambda^{pert} - \boldsymbol{b}^{pert}\right\|_2$ [2, 5]. This curve is shown in Fig. 8 for the first LOSA deconvolution problem described above with N = 50. Solutions on the left-hand side of the curve are under-regularized since they satisfy $\mathbf{A}_{\mathrm{OP}}\boldsymbol{x}_\lambda^{pert} = \boldsymbol{b}^{pert}$ accurately but are contaminated by large perturbations as

indicated by the large solution norm, $\left\|\mathbf{L}\boldsymbol{x}_{\lambda}^{pert}\right\|_2$. Points that lie on the right-side of the curve, on the other hand, correspond to over-regularized solutions that are smooth but no longer satisfy the original ill-posed problem. The best trade-off between smoothness and accuracy is usually found by inspecting solutions that lie near the corner of the L-curve, a time consuming process that demands intuition and knowledge of regularization on the part of the analyst.

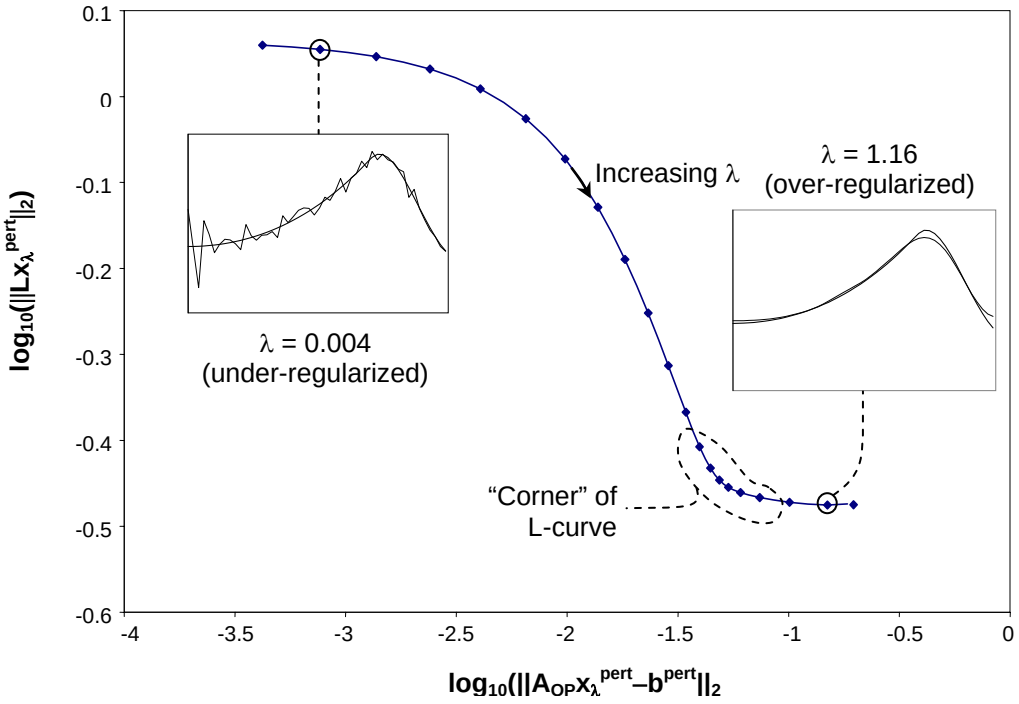

Fig. 8: Tikhonov L-curve for the first test problem with $N = 50$.

A more sophisticated way of choosing λ is based on the observation that, since $\varepsilon_{reg}(\lambda)$ and $\varepsilon_{pert}(\lambda)$ increase and decrease in a monotonic way with increasing λ, these errors can be balanced by using the value of λ that satisfies $\varepsilon_{reg}(\lambda^{\dagger}) = \varepsilon_{pert}(\lambda^{\dagger})$. As will be demonstrated later, $\lambda^{\dagger}$ also lies very close to the optimal level of regularization that minimizes $\varepsilon_{tot}(\lambda)$, $\varepsilon_{tot}(\lambda^{*}) = Min[\varepsilon_{tot}(\lambda)]$. Unfortunately, $\lambda^{\dagger}$ cannot normally be found

using Eq. (15) directly, since $\boldsymbol{b}^{pert}$ is known rather than $\boldsymbol{b}$ and $\boldsymbol{\delta b}$ individually. An estimate of $\|\boldsymbol{\delta b}\|_2$ is often available, however, usually from the variance of independently-measured sets of projected data. If this is the case $\lambda^{\dagger}$ can be approximated using the *discrepancy principle* [5, 10], which states that λ should be chosen so that

$$\left\|\mathbf{A}_{OP}\boldsymbol{x}_{\lambda}^{pert} - \boldsymbol{b}^{pert}\right\|_2 = \delta_e \geq \left\|\boldsymbol{\delta b}\right\|_2, \tag{15}$$

where δ_e is most often set equal to $\|\boldsymbol{\delta b}\|_2$. The left- and right-hand sides of Eq. (15) are estimates of the regularization and perturbations errors, respectively, projected into the vector space of $\boldsymbol{b}$. The discrepancy principle can be used to select the Tikhonov regularization parameter automatically by first substituting an estimate of $\|\boldsymbol{\delta b}\|_2$ into Eq. (15) and then solving for λ using a safe-guarded root-finding algorithm.

In some cases, however, an estimate of $\|\boldsymbol{\delta b}\|_2$ is unavailable, for example when the number of experimental trials that can be performed is limited. In this scenario, a recently-developed algorithm [4, 11] based on truncated singular value decomposition (TSVD) [5] can be employed to estimate the magnitude of the perturbation error contaminating the projected data. This procedure starts with the singular value decomposition of $\mathbf{A}_{\mathrm{OP}}$. Next, the useful rank of $\mathbf{A}_{\mathrm{OP}}$, p, is estimated by identifying the value of j where $\boldsymbol{u}_j^T\boldsymbol{\delta b}/s_j$ dominates $\boldsymbol{u}_j^T\boldsymbol{b}/s_j$ in the series $\{g_j = \boldsymbol{u}^T\boldsymbol{b}^{pert}/s_j, j = 1\ldots N\}$. Terms in the series having indices greater than the useful rank, i.e. $\{g_j, j > p\}$, are unimportant in the reconstruction of $\boldsymbol{x}$ but are instead the source of the perturbations, $\boldsymbol{\delta x}$, as described above. A smoothed solution, $\widetilde{\boldsymbol{x}}$, can thus be recovered by truncating these $N - p$ terms from the summation in Eq. (8),

$$\widetilde{\boldsymbol{x}} = \sum_{j=1}^{p} \frac{\boldsymbol{u}_j^T\boldsymbol{b}^{pert}}{s_j}\cdot\boldsymbol{v}_j. \tag{16}$$

which is then used to estimate $||\boldsymbol{\delta b}||_2$ by

$$\left\|\boldsymbol{\delta b}\right\|_2 \approx \left\|\boldsymbol{b}^{pert} - \widetilde{\boldsymbol{b}}\right\|_2 = \left\|\boldsymbol{b}^{pert} - \mathbf{A}_{\mathrm{OP}}\widetilde{\boldsymbol{x}}\right\|_2 . \tag{17}$$

Finally, this estimate of $||\boldsymbol{\delta b}||_2$ is substituted into Eq. (15), which in turn is solved for λ using a safe-guarded root-finding procedure.

Demonstration of Auto-Regularization Methods

The performance of the auto-regularization methods described above is compared to that of onion-peeling and Abel three-point deconvolution techniques by solving the two deconvolution test problems shown in Fig. 2. In order to simulate experimental flame conditions, projected data is contaminated with errors that are randomly-sampled from an unbiased Gaussian distribution having a standard deviation of $0.01\sqrt{20}$. Each element of the perturbed dataset, $\boldsymbol{b}^{pert}$, is then found by taking the average of 20 independent samples, and the corresponding standard deviation of the mean, σ_m, is given by $\sigma/\sqrt{20}$, where σ is the standard deviation of the sampled data. The expected value of σ_m is $E(\sigma_m)$ = 0.01, a typical value for LOSA experiments carried out on laminar flames [6].

The performance of the deconvolution techniques is measured by the root-mean-squared error of the deconvolved field distribution,

$$\varepsilon_{\mathrm{RMS}} = \frac{\left\| \boldsymbol{x}^{pert} - \boldsymbol{x} \right\|_2}{\sqrt{N}}, \tag{18}$$

for solutions obtained using different numbers of projections, N. (Note that N is the size of $\boldsymbol{x}$.) The onion-peeling, Abel three-point, and TSVD-based auto-regularization algorithm [6, 11] require only the projected dataset, $\boldsymbol{b}^{pert}$, to carry out the deconvolution. If the discrepancy principle is used to calculate λ directly, however, the analyst must provide an estimate of $\|\boldsymbol{\delta b}\|_2$, which in this problem is approximated by

$$\left\| \boldsymbol{\delta b} \right\|_2 \approx \sqrt{N}\sigma_m = \sqrt{\frac{N}{20}}\sigma. \tag{19}$$

The corresponding regularization parameter is then found by solving Eq. (15) with a safeguarded secant root-finding algorithm [9].

At each value of N, 20 independent sets of projected data are supplied to the deconvolution algorithms, and the averages of the resulting $\varepsilon_{\mathrm{RMS}}$ values are plotted in Figs. 9 and 10 for the first and second deconvolution test problems, respectively. (The Tikhonov regularization parameter found using Eq. (15) alone is denoted λ_{AR1}, while the one found using the TSVD-based auto-regularization algorithm [6, 11] is λ_{AR2}.) Figures 9 and 10 show that both auto-regularization schemes outperform onion-peeling and Abel three-point deconvolution at large values of N, and the Tikhonov solution obtained using λ_{AR1} is the most accurate over the whole range of N. In fact, the root-mean-squared errors of the Tikhonov solutions generally decrease as N increases, since the perturbation error is suppressed to the extent that the dominant error in the is caused by assuming a uniform $f(r)$ over each element, which diminishes with increasing N. Example deconvolutions obtained using $N = 50$ are shown in Figs 11 and 12.

The quality of the regularization parameter chosen by the two auto-regularization methods is assessed by plotting the perturbation, regularization, and total error as a function of λ for Tikhonov regularization performed on the first test problem using $N = 20$ and $N = 50$, as shown in Figs. 13 and 14, respectively. (Note that λ^* is larger for the $N = 50$ case compared to the $N = 20$ case in order to suppress the larger perturbation error.) Both algorithms find values of λ that are reasonably close to λ^* and $\lambda^\dagger$ for $N = 20$, although the value of λ found by substituting the estimate of $\|\boldsymbol{\delta b}\|_2$ found by replication directly into Eq. (15) is better than the one obtained through TSVD, which is why Tikhonov solutions calculated using λ_{AR1} are more accurate than those found using λ_{AR2} for small values of N, as shown in Figs. 9 and 10. These regularization parameters lie closer to λ^* and $\lambda^\dagger$ for the $N = 50$ case, however, since the predictions of $\|\boldsymbol{\delta b}\|_2$ obtained

by replication and by TSVD become more accurate with increasing N. Beyond this value of N, the performance of the two auto-regularization schemes is approximately equal.

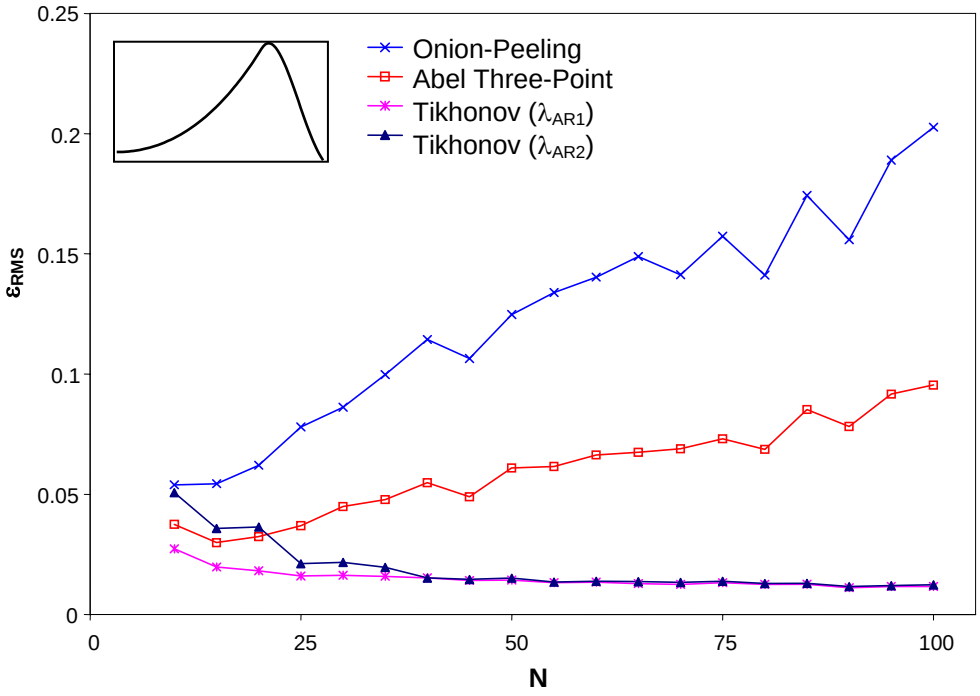

Fig. 9: Accuracy of different deconvolution techniques for the first test problem.

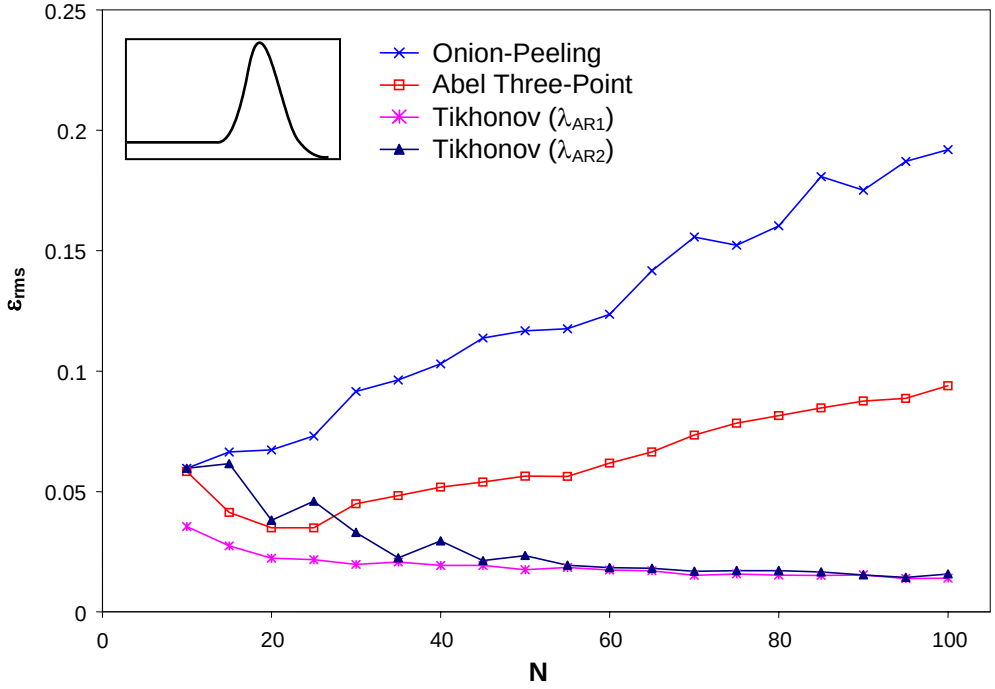

Fig. 10: Accuracy of different deconvolution techniques for the second test problem.

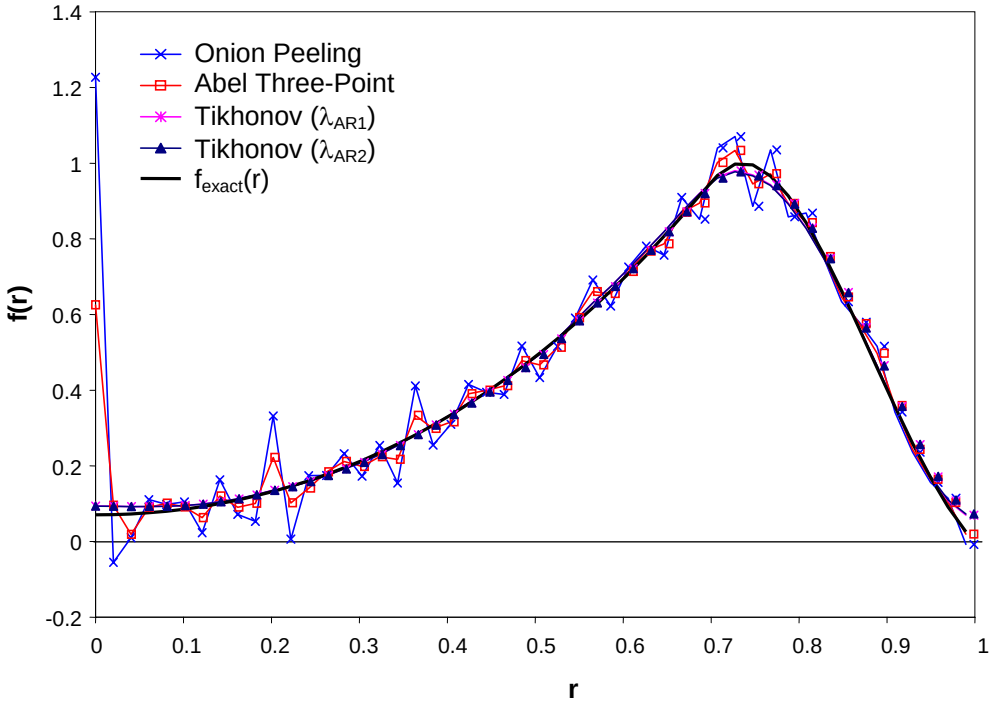

Fig. 11: Deconvolved field variable distributions for the first test problem, with $N = 20$.

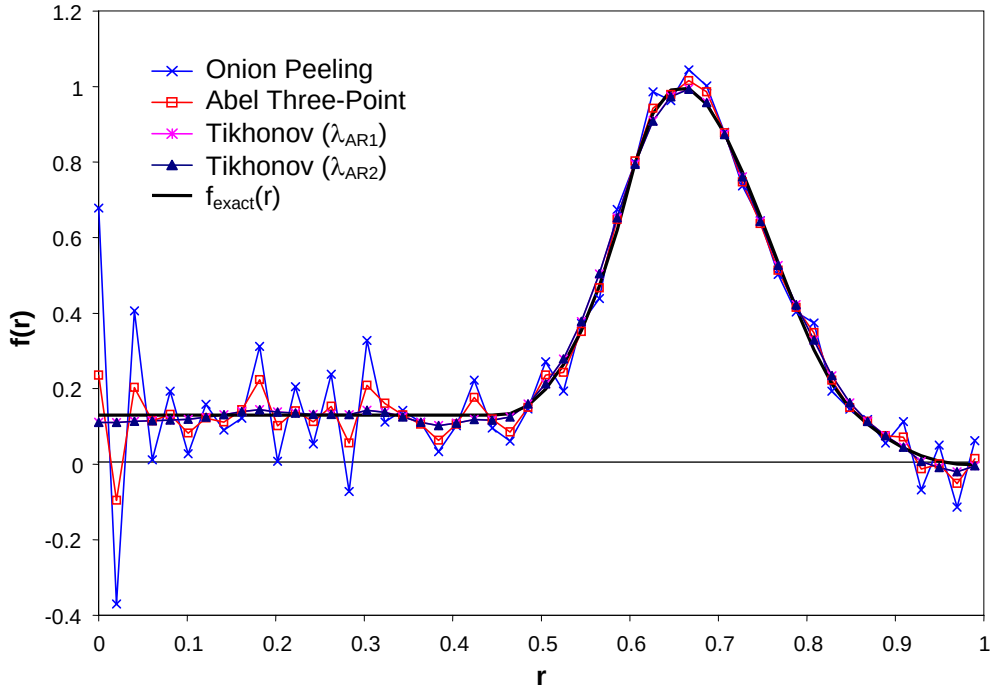

Fig. 12: Deconvolved field variable distributions for the second test problem, with $N = 50$.

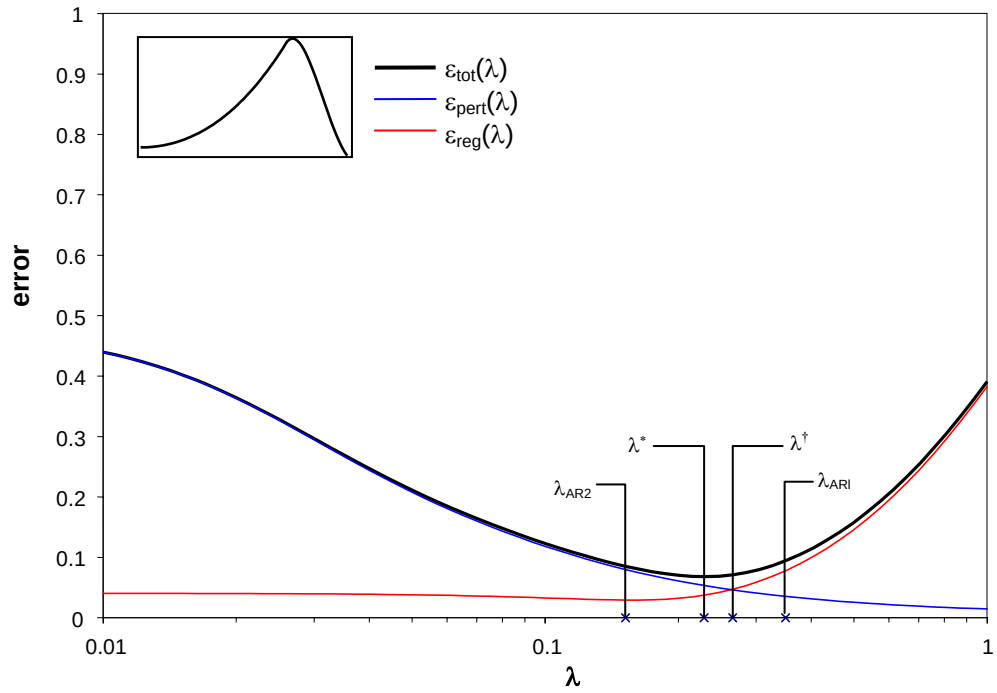

Fig. 13: Tikhonov deconvolution errors for the first test problem, with $N = 20$.

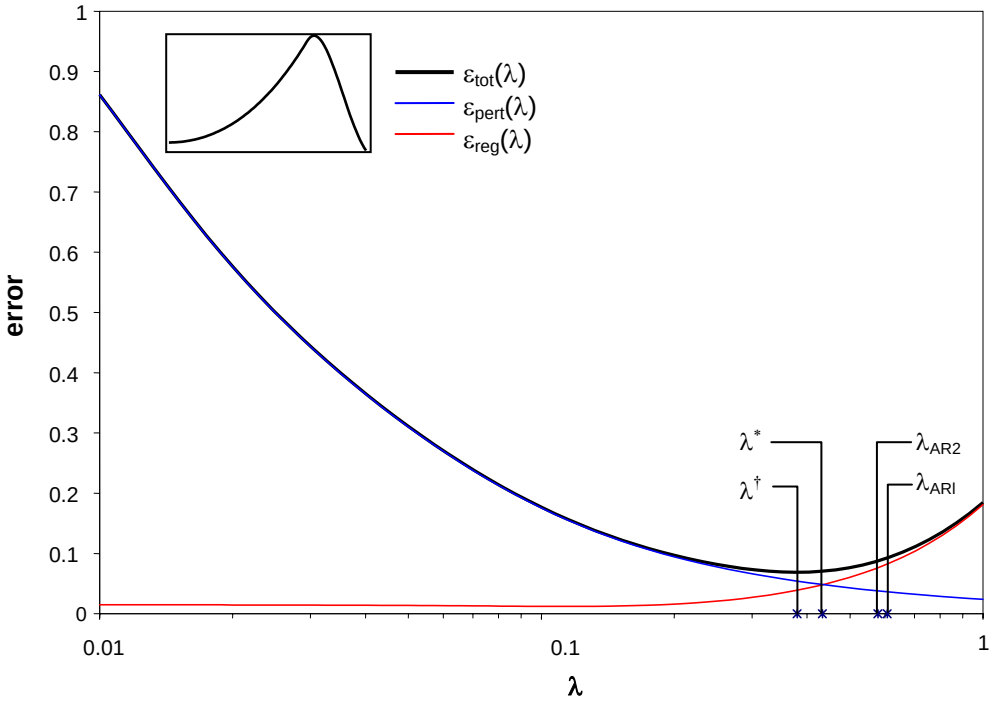

Fig. 14: Tikhonov deconvolution errors for the first test problem, with $N = 50$.

Conclusions

Tikhonov regularization is an effective way of solving axisymmetric flame deconvolution problems in which the projected dataset is contaminated with error, but the analyst must first identify a suitable regularization parameter. Traditionally, this is done manually by trial-and-error, a time-consuming process that demands experience and intuition of the analyst.

This paper presented two algorithms for finding the Tikhonov regularization parameter automatically. Both are based on the discrepancy principle, which uses an estimate of the error contamination to find a regularization parameter that gives a good trade-off between regularization error and perturbation error in the Tikhonov solution. In the first technique, the analyst provides an estimate of the error contamination directly to the algorithm, which is usually based on the variance of results obtained from repeated experimental trials. The second technique estimates the error directly using truncated singular value decomposition, which makes it ideal for situations where conducting repeated experiments is impractical.

Both algorithms provide solutions that are more accurate than those obtained by onion-peeling and Abel three-point deconvolution at moderate to high levels of flame-field discretization, and solutions obtained using the first auto-regularization scheme are superior to all others at all levels of discretization. Furthermore, since the regularization parameter is selected automatically, deconvolution is carried out quickly and efficiently without requiring any knowledge of regularization on the part of the analyst, making both algorithms ideal deconvolution tools for the combustion community.

References

[1] C. J. Dasch, One-Dimensional Tomography: A Comparison of Abel, Onion-Peeling and Filtered Backprojecton Methods, *Applied Optics*, Vol. 31, pp. 1146-1152 (1992).

[2] K. J. Daun, K. A. Thomson, F. Liu, and G. J. Smallwood, Deconvolution of Axisymmetric Flame Properties using Tikhonov Regularization, *Applied Optics*, in press.

[3] A. N. Tikhonov, Inverse Problems in Heat Conduction, *Journal of Engineering Physics*, Vol. 29, pp. 816-820 (1975).

[4] R. E. Jones and C. B. Moler, Automatically Regularized Nonnegative Solutions for Ill-Conditioned Linear Systems, *Proc. 2006 IPES*, (2006).

[5] P. C. Hansen, Rank-Deficient and Discrete Ill-Posed Problems, SIAM, 1998.

[6] K. A. Thomson, Ö. L. Güilder, E. J. Weckman, R. A. Fraser, G. J. Smallwood, and D. R. Snelling, Soot Concentration and Temperature Measurements in Co-Annular, Nonpremixed CH4/Air Laminar Flames at Pressures up to 4 MPa, Combustion and Flame, Vol. 140, pp. 222-232 (2005).

[7] J. Hadamard, Lectures on Cauchy's Problem in Linear Differential Equations, Yale University Press, 1923, as reported in [5].

[8] R. Gorenflo and S. Vessella, Abel Integral Equations: Analysis and Applications, No. 1461 in Lecture Notes in Mathematics, A Dold, B. Eckmann and F. Takens, Eds., Springer-Verlag, 1991.

[9] W. H. Press, S. A. Teukolsky, W. T. Vetterling, and B. P. Flannery, Numerical Recipes in C: The Art of Scientific Computing, 2nd Ed., Cambridge University Press (2002).

[10] V. A. Morozov, On the Solution of Functional Equations by the Method of Regularization, Soviet Math. Dokl., Vol. 7, pp. 414-417 (1966), as reported in [5].

[11] R. E. Jones, "Autoreg", an algorithm for computing automatically regularized nonnegative solutions for ill-conditioned linear systems, www.rejonesconsulting.com, (2006).